Erosion of the Subsurface Salinity Maximum of the Loop Current Eddies From Glider Observations and a Numerical Model

R. Sosa-Gutiérrez, E. Pallàs-Sanz, Julien Jouanno, Alexis Chaigneau, J. Candela, M. Tenreiro

JGR Oceans

RESEARCH ARTICLE
10.1029/2019JC015397

Key Points:
- The vertical structure of salinity is similar from one eddy to another, regardless of the detachment month from the LC
- The most important physical process that controls the salt budget in the LCEs' core is the vertical salinity diffusion
- The vertical salinity diffusion is driven by thermal convection due to cold and dry *Northerly* winds

Correspondence to:
R. Sosa-Gutiérrez,
esosa@cicese.edu.mx

Citation:
Sosa-Gutiérrez, R., Pallàs-Sanz, E., Jouanno, J., Chaigneau, A., Candela, J., & Tenreiro, M. (2020). Erosion of the subsurface salinity maximum of the Loop Current Eddies from glider observations and a numerical model. *Journal of Geophysical Research: Oceans*, *125*, e2019JC015397. https://doi.org/10.1029/2019JC015397

Received 17 JUN 2019
Accepted 5 JUN 2020
Accepted article online 16 JUN 2020

Erosion of the Subsurface Salinity Maximum of the Loop Current Eddies From Glider Observations and a Numerical Model

R. Sosa-Gutiérrez[1], E. Pallàs-Sanz[1], J. Jouanno[2], A. Chaigneau[2,3,4], J. Candela[1], and M. Tenreiro[1]

[1]Departamento de Oceanografía Física, Centro de Investigación Científica y de Educación Superior de Ensenada, Ensenada, México, [2]Laboratoire d'Études en Géophysique et Océanographie Spatiale (LEGOS), Université de Toulouse, CNES, CNRD, IRD, UPS, Toulouse, France, [3]Institut de Recherches Halieutiques et Océanologiques du Bénin (IRHOB), Cotonou, Benin, [4]International Chair in Mathematical Physics and Applications (ICMPAâUNESCO Chair), University of Abomey-Calavi, Cotonou, Benin

Abstract The erosion of the subsurface salinity maximum, signature of the Caribbean Subtropical UnderWater (SUW), within the Loop Current Eddy (LCE) Poseidon (August 2016 to July 2017) in the Gulf of Mexico (GoM) and the formation of the Gulf Common Water (GCW) during its journey westward, was observed using glider data. Most of the dilution of the SUW high-salinity core within Poseidon occurs during late autumn and winter associated with *Northern* winds and mixed-layer deepening. The physical processes that contribute to salt dilution of the SUW inside the LCEs' core are investigated using a numerical regional model. The analysis of the salt budget in a long-lasting numerical LCE and a composite analysis of sixteen LCEs reveal that the salinity trend is mostly explained by the vertical salinity diffusion. Cold and dry *Northern* winds during the first winter drive strong negative net heat fluxes that trigger turbulent flux of salt into the LCEs' thermostad and dilution of the SUW high-salinity core below. The vertical salinity diffusion continues homogenizing the salinity in the upper ocean until the vertical gradient of salinity is negligible. As a result, SUW is transformed to precursor of GCW that is ultimately diffused to surrounding waters in the western GoM. Although the contribution of advection to the salinity trend above the isopycnal of 1,026 kg m^{-3} is of second order, below is the most important process driving loss of salinity, presumably due to, eddy-eddy interactions during LCEs' westward propagation and eddy pumping (upwelling) during the LCEs' decaying phase along the western slope.

Plain Language Summary This study shows that the vertical salinity diffusion (ZDF) is the main physical process that controls the erosion of the Caribbean Subtropical UnderWater high-salinity core within the Loop Current Eddies during the first winter of their life cycles in the Gulf of Mexico. The ZDF during winter is associated with negative heat fluxes that are driven by thermal convection mixing through the passage of cold and dry fronts (Northerly winds). It is suggested that the formation of the Gulf Common Water is due to the progressive erosion of the high-salinity core of the Loop Current Eddies during their journey to the west of the Gulf of Mexico.

1. Introduction

The large-scale water mass characteristics in the central and western Gulf of Mexico (GoM) consist of four main water masses in the first ~1,500 m depth (Elliott, 1982; Vidal et al., 1994): the Gulf Common Water (GCW; ~36.4, ~22°C) found above 200 m, the Suptropical UnderWater (SUW; >36.5, ~23°C) at depths between 200 and 300 m, the Tropical Atlantic Central Water (TACW; ~35.2, ~10°C) at depths between 300 and 600 m, and the Antarctic Intermediate Water (AAIW; ~34.9, ~6°C) below. The circulation in the GoM is dominated by mesoscale dynamics, with the presence, in particular, of large anticyclonic eddies shed by the Loop Current (LC). These Loop Current Eddies (LCEs) propagate westward through the GoM along a broadband of west-southwest paths (Dussin et al., 2016; Hamilton et al., 1999) and dissipate at the western boundary of this semienclosed basin (Vukovich & Crissman, 1986; Vukovich, 2007).

The LCEs play a dominant role in setting the water mass properties of the GoM. The LCE shedding process leads to advection of SUW in the interior of the GoM, contributing to the salinization of the basin. This water

mass, characterized by salinities exceeding 37 (O'Connor et al., 2005), is formed in the subtropical North Atlantic Ocean due to the excess of evaporation over precipitation (Qu et al., 2011) and subducts into the thermocline by Ekman pumping (Qu et al., 2016). The SUW is then transported toward the GoM by the tropical western boundary current system formed by the Caribbean and Yucatan currents. In general, mesoscale eddies participate to the dynamical balance of the oceans and can affect the physical and biological properties away from their regions of generation. Water parcels with large temperature and salinity anomalies are trapped into the interior of individual eddies; hence, they transport heat and salt due to their movement, typically westward (Dong et al., 2013).

Based on historical in situ data, several studies have described the horizontal and vertical thermohaline structure of the LCEs in the central and western GoM (Cooper et al., 1990; Elliott, 1982; Meunier et al., 2018; Rudnick et al., 2015; Vidal et al., 1994; Vukovich & Crissman, 1986). They reveal that LCEs have typical radii of the order of 100–150 km, vertical extents of about 1,000 m depth, maximum swirl speeds of 2 m s^{-1}, horizontal propagation velocities of 2–5 km day^{-1}, and exhibit different thermohaline structures depending on their location in the GoM. A strong subsurface salinity maximum (>36.5 at 22.5°C) has been observed in LCEs near their formation region (LC system) and central GoM (Elliott, 1982; Vidal et al., 1994). Recently, Meunier et al. (2018) using high-resolution glider data confirmed the presence of a subsurface salinity maximum higher than 36.9 within a given LCE in the central GoM that contrasts with the surrounding water characteristics. On the other hand, LCEs sampled in the western GoM present largely intact signals of the SUW (36.6–36.65; Brooks, 1984; Hamilton et al., 2018) or diluted high-salinity cores (<36.40 and <22.5°C Vidal et al., 1994). Hence, SUW is progressively eroded and transformed to GCW during the westward propagation of the LCEs within the GoM and/or at the eddy graveyard (Biggs, 1992) by LCE-slope interactions (Vukovich & Waddell, 1991). A very recent observational work shed some light on LCEs' decay using 25 years of altimetry (Meunier et al., 2020). The authors report that nearly two thirds of the total heat (and salt) content of the LCEs is released to surrounding waters through (submesoscale) lateral diffusion after 130 days, that is, about 2 months before they reach the western GoM. Their results question the previously accepted idea that this region is a graveyard for LCEs (Biggs, 1992).

We are mainly interested in the water mass transformation occurring in the upper 300 m (above the isopycnal of 1,026 kg m^{-3}) and within the core of the LCEs, a process that may not directly have an effect on the total heat and salt content of the eddies. Here and throughout the manuscript we define the core of the LCEs as the region enclosed within a 30 km radii from the center, which is consistent with the first baroclinic Rossby radius of deformation observed in the GoM (30–50 km; Chelton et al., 1998). We focus in the central region of the trapped fluid within the LCEs far away from their boundary that approximately represents the transition between SUW and GCW. The decay of warm-core rings driven by lateral diffusion of heat and salt (Meunier et al., 2020) is, therefore, out of scope.

The aim of this study is to better understand how SUW is transformed to GCW, specifically determine which physical mechanisms erode the subsurface salinity maximum of the LCEs the most. For that purpose, (1) we took benefit of a set of four glider missions designed to sample a LCE (called Poseidon) along its trajectory from central to western GoM in 2016–2017, giving insights on the timing of the SUW transformation, and (2) we analyzed outputs of a 20 year long regional high-resolution ocean model in order to better understand the processes at play in the observed evolution of the salinity properties in the core of the LCEs. In particular, we chose the longest-lasting LCE (~2 years) to have more details about the salinity evolution along its westward journey within the GoM.

The paper is organized as follows. Glider observations, as well as the regional model and inferred diagnostics, are described in section 2. Results are presented in section 3 for the glider observations, section 4 for the model, and section 5 for the available heat and salt anomaly contents within the LCEs computed using gliders observations and the regional model. Discussion and concluding remarks are given in section 6.

2. Material and Methods

2.1. Glider Data

The "Grupo de Monitoreo Oceanográfico con Gliders" (GMOG) launched a monitoring program of the mesoscale and submesoscale flow structures in the central and western GoM using autonomous

underwater gliders. GMOG monitored the LCE Poseidon from 6 August 2016 (4 months after its detachment) until its dissipation in the western GoM (25 July 2017), for about 1 year, along with four glider missions (0003–0006) with three autonomous underwater vehicles type Seaglider (Serial Numbers SG623, SG624, and SG625). The three GMOG gliders were in particular equipped with a free-flow SeaBird Conductivity Temperature Depth (CTD) probe (CT-Sail) acquiring data from the surface down to at least 1000 m depth with a sampling frequency of 0.1 Hz. Each GMOG gliders' CTD was calibrated in different period, for example, the CT sails mounted on SG623 and SG624 were calibrated on 1 June 2015 and the one on SG625 on 2 November 2016. All the CTDs used during the four missions were calibrated within two years as recommended by the manufacturer. The compass of SG624 stopped recording data on 22 December 2016, and the glider started drifting with the current but continued diving along a sawtooth trajectory measuring the water column.

For this study we used a total of 1,834 dive cycles with a spatial resolution of 2–5 km and a vertical resolution of 0.5–2 m that depends on ambient currents, the dive angle (i.e., pitch), and buoyancy of the gliders. The temperature and vertical salinity profiles were vertically (linearly) interpolated every 0.5 m depth along the gliders' sawtooth trajectory. Because Seaglider uses unpumped CT sail, salinity is corrected using the method of Garau et al. (2011) to remove salinity spikes due to thermal lag effects on the conductivity cells. This effect is especially important across strong vertical temperature gradients such as at the base of the thermocline. The depth-averaged velocity for each dive cycle is computed from the difference of the glider displacement through the water and the GPS-measured displacement at the beginning and end of the dive (Rudnick et al., 2015). The glider data used in this work can be freely visualized, and contextualized with satellite imagery, on the GMOG website (https://gliders.cicese.mx/).

2.2. Regional Simulations

2.2.1. Numerical Setup

The regional numerical model used in this study is NEMO (Madec & the NEMO team, 2016), which solves the primitive equations on a domain extending from 98°W to 78°W and from 14°N to 30°N, and 75 fixed vertical levels (with 12 levels within the first 20 m and 24 levels in the upper 100 m to better resolve the mixed-layer processes). The temporal resolution of the outputs of this simulation is 1 day, and the horizontal resolution is (1/12)° grid, corresponding to a $\Delta x = 8.4$ km in the GoM, which is suitable to resolve mesoscale dynamics in the studied region. The model has been integrated from 1 January 1993 to 31 December 2012. The horizontal advection scheme used for the temperature and salinity is the Total Variance Dissipation (TVD) scheme, and the horizontal diffusion is parameterized as a Laplacian isopycnal diffusion, with a coefficient of 135 $m^2\,s^{-1}$. The momentum advection scheme is the third-order upstream biased (UP3) with no explicit horizontal diffusion. The vertical diffusion of momentum and tracers is computed with a Generic Length Scale (GLS) scheme with a $k-\varepsilon$ turbulent closure (Reffray et al., 2015; Umlauf & Burchard, 2003). At the ocean floor, quadratic bottom friction is applied with a bottom drag coefficient of 10^{-3} .

The model is forced at the open boundaries with daily outputs of the global MERCATOR reanalysis GLORYS2V3. At the surface, the atmospheric fluxes of momentum, heat, and freshwater are computed using bulk formulation (Large & Yeager, 2004) and the DFS5.2 forcing set (Dussin et al., 2016), which consists in 3 hr fields of wind speed, air temperature, and humidity, and daily fields for longwave and shortwave radiation and precipitation. The model uses a monthly climatological runoff (Dai & Trenberth, 2002) prescribed near the river mouths as a surface freshwater flux. There is no temperature and salt relaxation in our simulation.

2.2.2. Salt Budget at the Eddy Scale

One way to investigate the evolution of the subsurface salinity maximum in the model is to statistically study the salt budget within the core of westward propagating numerical LCEs. This implies (a) to automatically identify and track the LCEs in the GoM simulations and (b) to provide an exact (online) estimation of the different terms of the salt budget.

2.2.2.1. Eddy Detection

First, LCEs are identified using a slight modification of the eddy detection method reported in Chaigneau et al. (2009). This algorithm consists in searching, on each daily Sea Level Anomaly (SLA) maps, the local maxima of SLA, which are associated with the centers of anticyclonic eddies. For each detected center, the algorithm searches for the outermost closed SLA contour, which is considered as the anticyclonic eddy edge. In this

study, LCEs are detected using Absolute Dynamic Topography (ADT) altimetry maps, and their edges correspond to the closed ADT contour along which the averaged azimuthal velocity is maximum. This method, also used by Laxenaire et al. (2018), reduces the number of spurious eddies identifications and blends both geometrical (Chaigneau et al., 2009) and dynamical (Isern-Fontanet et al., 2003) detection criteria.

Second, LCEs are temporally tracked using the eddy-tracking algorithm developed by Pegliasco et al. (2015). Basically, this algorithm reconstructs eddy trajectories searching for eddy edge intersections between consecutive maps. Readers interested in more details on this eddy-tracking algorithm are referred to Pegliasco et al. (2015). The eddy detection and tracking algorithms were applied on two databases: (i) the daily ADT maps (0.25° × 0.25°) from 1993 to 2017 distributed by Copernicus Marine and Environment Monitoring Service (CMEMS; https://www.copernicus.eu/en) and (ii) the daily SSH maps obtained using NEMO (1993–2012). In this study, we only retain LCEs having radii larger than 40 km and lasting more than 180 days in the GoM. As a result, only 16 numerical LCEs from the total of 34 detected with the algorithm are analyzed in this study. Over 44% of the 34 LCEs were separated in March, April, May, and June in agreement with the eddy-shedding statistics obtained from a 33 year satellite imagery (Vukovich, 2007) but contrasting with the 26% reported in Hall and Leben (2016). In the CMEMS database, we only aim to detect and track the LCE Poseidon, while in NEMO database we analyzed the sixteen numerical long-lived LCEs.

Following the methodology of Chaigneau et al. (2011), we estimate the available heat and salt content anomalies, AHA and ASA, respectively, that the LCEs transport into the western GoM,

$$AHA = \int \rho C_p \theta' \, dA, \tag{1}$$

and

$$ASA = 0.001 \int \rho S' \, dA, \tag{2}$$

where $\rho =$ 1,026 kg m^{-3} is a mean density, $C_p =$ 4,200 J kg^{-1} °C^{-1} is the specific heat capacity, θ' and S′ are the anomalies for the temperature and salinity evaluated at each depth, respectively, and integrated over the area delimited by the edge of the LCE. For the computed AHA and ASA from glider observations, the temperature and salinity anomalies were estimated using a mean vertical profile of T/S (1993–2017) obtained from the updated climatology of the GoM reported in Portela et al. (2018), whereas for the computed AHA and ASA from the model, we used a T/S climatology obtained from the 20 years NEMO simulation.

2.2.2.2. Salt Balance

The Eulerian salt balance equation reads as follows:

$$\frac{\partial S}{\partial t} = \underbrace{-u\frac{\partial S}{\partial x} - v\frac{\partial S}{\partial y}}_{HAD} \underbrace{- w\frac{\partial S}{\partial z}}_{ZAD} + \underbrace{\frac{\partial}{\partial x}\left(k_h \frac{\partial S}{\partial x}\right) + \frac{\partial}{\partial y}\left(k_h \frac{\partial S}{\partial y}\right)}_{HDF} + \underbrace{\frac{\partial}{\partial z}\left(k_z \frac{\partial S}{\partial z}\right)}_{ZDF} + \underbrace{(E - P - R)S}_{FLX}, \tag{3}$$

where S is the model's salinity, (u, v, w) are the velocity components in the zonal, meridional, and vertical directions, respectively, k_h is the horizontal diffusion coefficient ($k_h = 135$ m^2 s^{-1}), k_z is the vertical diffusion coefficient (k–ε scheme; Reffray et al., 2015; Umlauf & Burchard, 2003), E is evaporation, P is precipitation, and R is the river runoff (kg m^{-2} day^{-1} or mm day^{-1}). The left-hand side of Equation 3 represents the rate of change of salinity whereas the forcing terms for salinity indicated on the right-hand side (RHS) correspond to the horizontal (HAD) and vertical (ZAD) salinity advection, the horizontal (HDF) and vertical (ZDF) salinity diffusion, and the freshwater fluxes (FLX), which are only occurring at the sea surface and, therefore, are implicitly divided by the depth of the uppermost level. Notice that the turbulent entrainment at the base of the mixed layer (Camara et al., 2015; Da-Allada et al., 2017)

$$\frac{1}{h} w_e (SSS - S_{z=-h}),$$

where w_e is the entrainment velocity, SSS is the sea surface salinity, and $S_{z=-h}$ is the salinity at $z = -h$, is not included explicitly in the Equation 3. The turbulent closure used in NEMO is the GLS scheme and

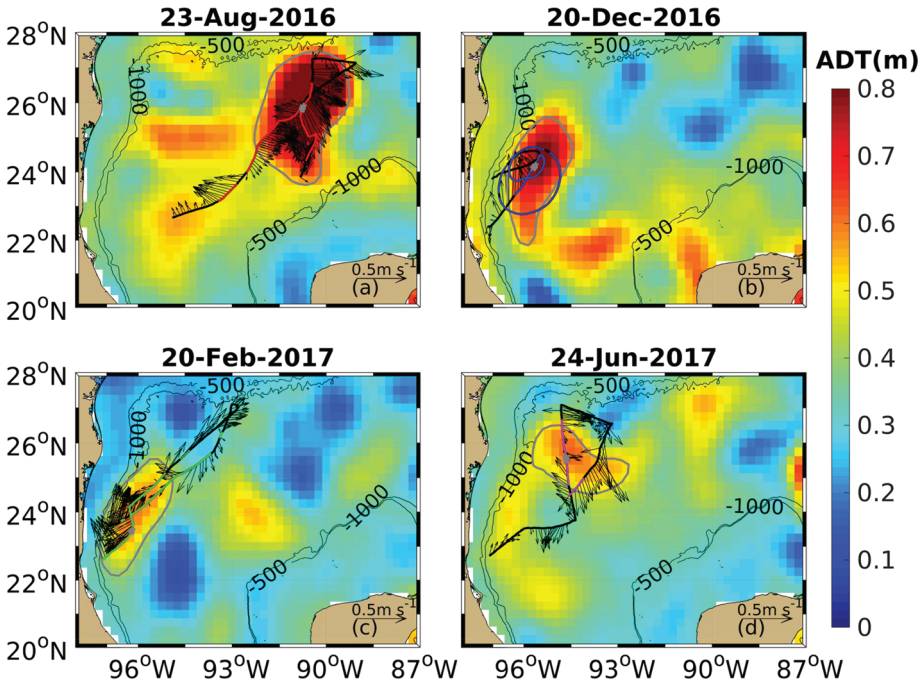

Figure 1. Maps of Absolute Dynamic Topography (ADT; m) at selected days from August 2016 to July 2017 with superimposed glider's trajectories (black lines): (a) 23 August 2016 (Mission 0003), (b) 20 December 2016 (Mission 0004), (c) 20 February 2017 (Mission 0005), and (d) 24 June 2017 (Mission 0006). The location of the vertical profiles obtained at the selected days is indicated with gray five-pointed stars in each panel. Colored lines in panels (a)–(d) indicate the locations where the gliders surface into the LCE Poseidon. Gray closed contours are the edges of the LCE Poseidon and the black arrows are the depth-averaged velocity ($m\,s^{-1}$) obtained from glider's flight.

gives the vertical diffusion coefficient in the whole water column. Thus, turbulent entrainment is implicitly included in the term of vertical diffusion of salinity, ZDF (Equation 3).

Salinity budgets have been widely used by several authors, using observations and models, to determine the most important physical processes driving local rate of salinity changes (Akhil et al., 2014; Camara et al., 2015; Da-Allada et al., 2013, 2017; Foltz et al., 2004; Qu et al., 2011).

The different terms in Equation 3 where computed online in order to ensure a closed balance and exact estimation of the nonlinear terms; and horizontally averaged (offline) within a 30 km radii from the LCE centers at each vertical grid point of the model. An exception is the term accounting for *FLX*, which is only computed for the uppermost depth level. The salinity budget was computed following 16 westward propagating numerical LCEs lasting more than 180 days. In order to determine the temporal variability of the salt balance terms in the LCE cores, this averaging process is repeated daily along each of the sixteen long-lived LCE trajectories. The residual term (*Res*) is defined as the difference between the salt trend ($\partial S/\partial t$) and the sum of the forcing terms

$$Res = \frac{\partial S}{\partial t} - RHS,$$

where

$$RHS = (HAD + ZAD + HDF + ZDF + FLX),$$

and informs about the salt balance equation error associated with the deformation of the LCEs (and the change of the control volume) during their westward propagation. By computing the salt budget only within a 30 km radii from the LCE centers, we reduce (i) the residual effect of LCEs' shape variability

Table 1
GMOG's Glider Missions: Mission ID, Period of Measurements, and the Total Dive Cycles per Mission

Mission ID gilder	Mission period	Dive cycles
0003-623	06-Aug-2016 to 07-Nov-2016	582
0004-623	09-Dec-2016 to 11-Mar-2017	429
0005-624	12-Feb-2017 to 01-May-2017	483
0006-625	27-May-2017 to 25-Jul-2017	340

and (ii) the effect of the horizontal diffusive processes because the horizontal gradients of salinity, in this control volume, are weak.

3. Observed Thermohaline Structure of the LCE Poseidon

First, the evolution of the thermohaline structure of a given LCE (Poseidon) using glider data is described, focusing on its vertical salinity structure. The LCE Poseidon detached from the LC on 15 April 2016 (Meunier et al., 2018). It has been sampled during four glider missions from August 2016 to July 2017 (Figure 1 and Table 1). Three different gliders from the GMOG's fleet (SG623, SG624, and SG625) were used to perform eight sections across Poseidon from the central (Mission 0003; Figure 1a) to the western GoM (Missions 0004–0006; Figures 1b–1d). Piloting efforts ensured the gliders to cross Poseidon along its largest thermohaline gradients or perpendicularly to the surface geostrophic current retrieved from daily altimetry. Mission 0004 was an exception because the glider's compass stopped recording, and the glider started to drift clockwise with the mean current but still profiling vertically along a sawtooth trajectory. Hence, the depth-averaged current during Mission 0004 is not available because the pitch, roll, and heading data could not be recovered.

The temporal evolution of salinity and temperature as a function of depth, wind speed over Poseidon, and geostrophic eddy kinetic energy (EKE), computed from altimetry (along the contour of maximum azimuthal velocity), are shown in Figure 2. Only data within the edge of Poseidon are shown, which has been identified using the eddy detection method (see details in section 2.2.2.1). The vertical thermohaline structure of Poseidon during its early life cycle (August 2016; Figures 2b and 2c (0003)) is characterized by a strong signature of the Caribbean SUW located between the isopycnals of 1,024.5 and 1,026 $kg\,m^{-3}$, with a high-salinity core above >36.9 and temperatures of ~23°C (Figures 2b and 2c (0003) and 3). This eddy is consistent with an intense LCE in its young phase, with maxima EKE reaching up to 0.1 $m^2\,s^{-2}$ (Figure 2d (0003)). At this time, a layer with homogeneous temperature (thermostad) and salinity (halinostad) is observed between the seasonal thermocline located near 30 m and the permanent thermocline located near 200 m. In the upper 30 m, we observe a layer of warmer (>28°C) and saltier waters maintained by strong air-sea heat fluxes and increased evaporation during August (summer). By the end of Mission 0003 (late October) the mixed-layer of Poseidon deepens down to ~75 m (Figure 2b (0003); dashed black line) associated with the passage of the first Northern winds of the season in the GoM and its EKE starts to decrease along its propagation westward (Figure 2d (0003)).

In late autumn (December, beginning of Mission 0004, Figure 2), the surface waters get cooler and fresher, and the Northern winds are intense. The seasonal thermocline is eroded, and the Poseidon mixed-layer deepens down to 150 m, near the base of the mixing layer (Figure 2c (0004)). Interestingly, there is a decrease of salinity of the high-salinity core along with an increase of salinity within the thermostad between 30 and ~200 m (Figures 2b and 2c (0004) and 3), suggesting that efficient mixing is occurring in the upper 300 m.

On average, the largest salinity erosion of up to 0.4 occurs within the core of the Caribbean SUW between 200 and 300 m depth (Figure 3b). LCE Poseidon separated in April 2016 and experienced autumn and early winter before reaching the western Gulf continental slope (Figure 2a). On 20 December, the compass of the glider disconnected and the glider started to drift clockwise with currents, moving along the edge of the LCE Poseidon for almost two complete revolutions of the glider.

The high-salinity core of the Caribbean SUW continues to dilute during winter and early spring (December to March, Mission 0004 and first half of Mission 0005; Figures 2b and 3b) and spring (April, second half of Mission 0005). These dilutions of the SUW coincide with the periods during which the LCE Poseidon interacted with the western Gulf continental slope and the glider was away from the center ($r > 0.7$; Figure 2a).

Due to sampling issues, since late January 2017 until the end of Mission 0004, the glider flew near the periphery of the LCE Poseidon lacking the subsurface salinity maximum of the SUW (Figure 2b). At the beginning of Mission 0005, a salinity maximum above 36.8 at ~175 m is observed again as the glider entered into the core of the LCE Poseidon (Figure 2a). In summer 2017 (June, Mission 0006), the salinity maximum is reduced to ~36.7 (Figure 2b (0006)) with an averaged reduction of ~0.2 between Missions 0005

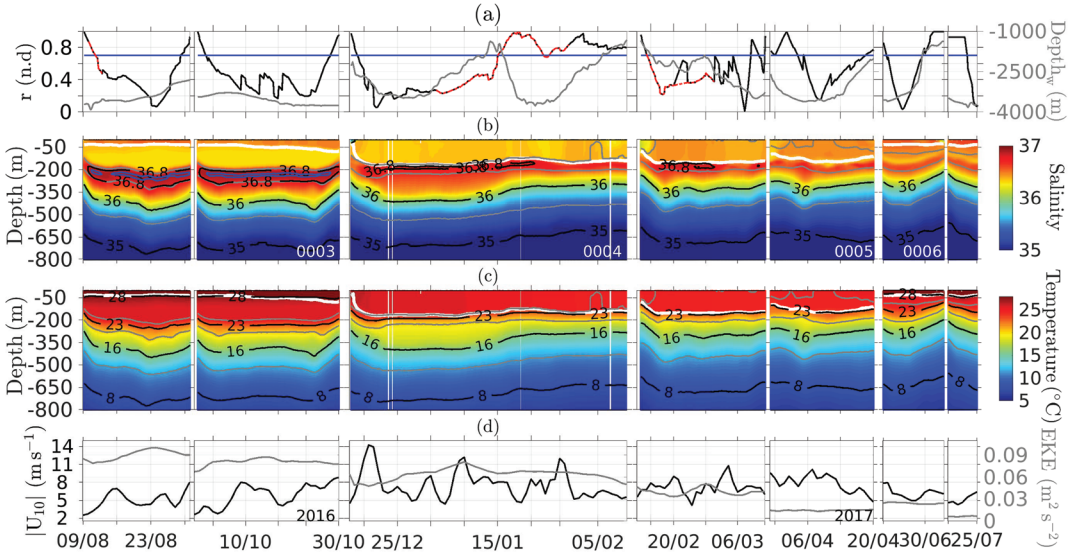

Figure 2. Time evolution during a year of Poseidon's life span of (a) the glider's location relative to the center of the eddy ($r = d/\mathscr{R}$; d is the distance between glider's location and eddy's center and $\mathscr{R}$ is the eddy's radius) and the water column depth (Depth$_w$; m) of measurements (black and gray lines, respectively), (b) salinity, (c) temperature (°C) as a function of depth, and (d) wind speed(m s^{-1}; black line), and eddy kinetic energy (EKE; m^2 s^{-2}; gray line) inside the LCE Poseidon. Red lines in (a) indicate the time periods of LCE-slope interactions defined here as the time when the periphery of the eddy (computed following Chaigneau et al., 2009) crosses over the isobath of 500 m. In (b) and (c), the dashed white lines represent the mixed-layer depth, the gray thick contours are the isopycnals of 1,024.5, 1,026, and 1,027 kg m^{-3}, the black thick contours represent the isohalines of 35, 36, and 36.8 and the isotherms of 8°C, 16°C, 23°C, and 28°C, respectively; and the blue contours in (b) are the isohaline of 36.9.

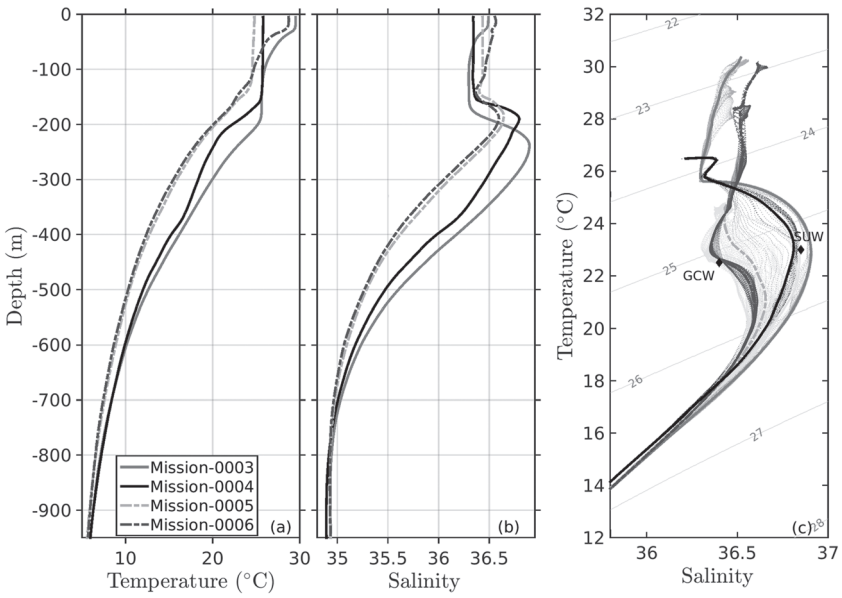

Figure 3. Mission-averaged vertical profiles inside LCE Poseidon: (a) temperature (°C) and (b) salinity. Each mission is color coded: Mission 0003 (gray), Mission 0004 (black), Mission 0005 (light gray), and Mission 0006 (light black). (c) Temperature-salinity (T-S) diagram inside LCE Poseidon of each mission (color-coded dots as in legend). The colored thick lines are the average T-S diagram of each mission and the black diamonds represent the mean T-S values for the Caribbean Subtropical UnderWater (SUW) and Gulf Common Water (GCW). Only data collected at the glider's locations relative to the center (r) below 0.7 are considered in the average to avoid contamination with anomalous salinity and temperature profiles of the periphery of the LCE Poseidon. T-S profiles obtained at time periods of eddy-slope interactions (red line in Figure 2a) are also removed from the average.

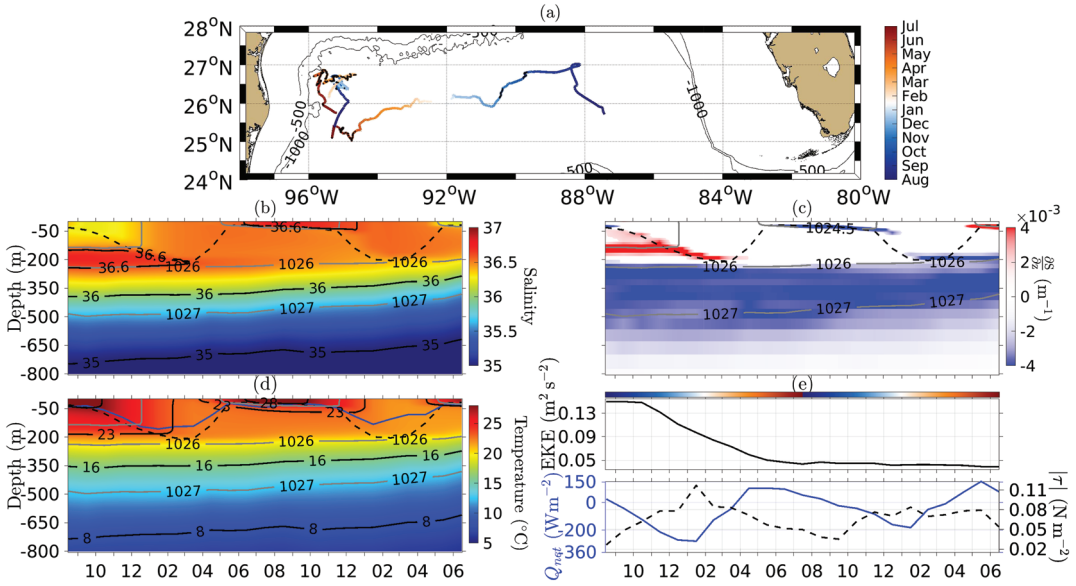

Figure 4. Case study of the longest-lived numerical LCE detached in August. Time evolution of (a) time color-coded trajectory of the LCE, (b) salinity, (c) vertical salinity gradient (m^{-1}), (d) temperature (°C), and (e) eddy kinetic energy (EKE, $m^2\,s^{-2}$; black line), net heat fluxes Q_{net} ($W\,m^{-2}$; blue solid line) and wind stress magnitude ($|\tau|$ ($N\,m^{-2}$); black dashed line); averaged within a 30 km radii from the LCE center. EKE is computed within the edge of the eddy (see section 3) and not over the radius of 30 km. The black points in (a) represent the locations of the LCE centers when their edge's cross over the isobath of 500 m. The dashed black lines in panels (b)–(d) represent the mixed-layer depth and the gray thick contours are the isopycnals of 1,024.5, 1,026, and 1,027 $kg\,m^{-3}$. Black thick contours in (b) and (c) are the isohalines of 35, 36, and 36.6 and the isotherms of 8°C, 16°C, 23°C, and 28°C, respectively. Blue thick line in panel (d) is the parameterized convective depth (Equation 4). The color bar in (e) represents the same time color coding used for the trajectory shown in (a).

(Figure 3b; light gray dashed line) and 0006 (Figure 3b; light black dashed line). This salinity difference is weaker than the decrease of salinity observed between Missions 0003 and 0004 (Figure 3b; gray and black lines). In summer 2017, surface warming restratifies the upper ocean leading to the formation of the seasonal thermocline at about 30 m depth (Figure 2b (0006); black line).

The T-S diagrams for the four missions clearly show a transformation of the Caribbean SUW to GCW within a year between Missions 0003 and 0006 (Figure 3c; black diamonds). We also note that the permanent thermocline of Poseidon gets shallower along its journey within the Gulf (Figures 2b and 2c, and 3a and 3b). This upward displacement of the isopycnals is suggestive of eddy decay. The spin down of the eddy is supported by the reduction of the depth-averaged velocity obtained from glider's flight data (see black arrows in Figure 1) and the EKE reduction (Figure 2d). The dilution of the high-salinity core during the Poseidon lifetime is strongly pronounced in the transition to Mission 0004 on winter (December to February), a period with very intense *Northern* winds over the GoM (Zavala-Hidalgo et al., 2014) that could play a key role in this erosion. The physical processes that could drive the erosion of the deep salinity maximum are investigated in the following section using the NEMO simulation.

4. Salinity Balance: Insights From a Regional Ocean Model

The 20 year long regional simulation is now used (i) to determine whether the fate of the salinity maximum observed for Poseidon using gliders is characteristic of most of the anticyclonic eddies that detach from the LC and (ii) to better understand the processes and timing of the erosion of the SUW. During the period of simulation (1993–2012), 16 LCEs lasting more than 180 days were identified. The salinity evolution and salt budget within the core of the LCEs are presented for both, a case study of longest-lived LCE (~2 years) and a composite LCE computed from the seasonal average of the 16 identified LCEs. The long-lived unusually coherent numerical LCE was able to maintain its integrity via merging processes with surrounding mesoscale anticyclonic eddies (not shown).

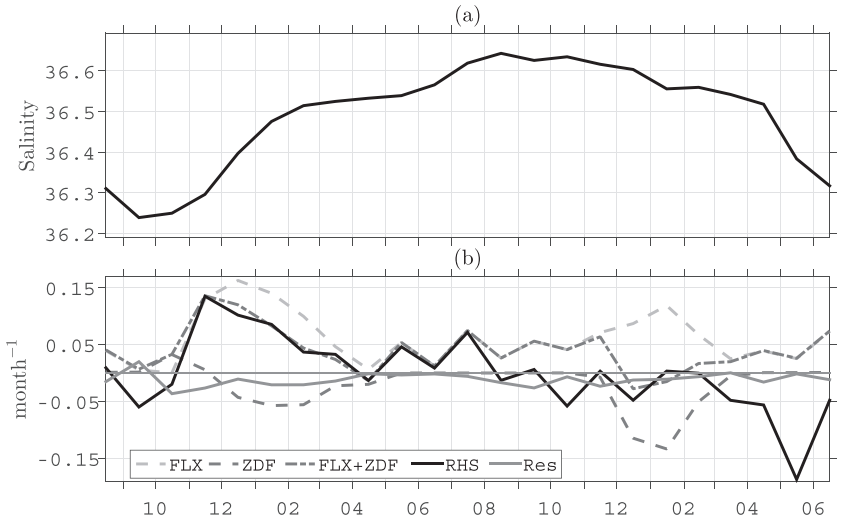

Figure 5. Time evolution of the vertical and horizontal average of (a) salinity and (b) the freshwater terms (FLX), vertical salinity diffusion (ZDF), right-hand size (RHS), and residual (*Res*), of the long-lived numerical LCE, within a 30 km radii from the LCE and from surface to 50 m depth. Line styles are described in the legend.

4.1. Case Study of the Longest-Lived LCE

In agreement with the observations, the longest-lived simulated LCE is characterized at the beginning of its life cycle by a subsurface salinity maximum (>36.6) associated with the Caribbean SUW (Figure 4b). This maximum, centered at ~200 m, is slightly shallower than the observed one during the early life of Poseidon (240 m; Figure 2b (0003)). Such differences may be attributed to a slight bias in the North Atlantic Subtropical water mass prescribed at the lateral boundaries of the regional model. Indeed, the vertical thermohaline structure of detached LCEs may vary from one eddy to another. The differences in EKE are also significant, with maximum initial values of 0.1 and 0.15 $m^2\,s^{-2}$ for Poseidon and the case study, respectively. The rate of decay (EKE reduction) being similar for both ($4–5 \times 10^{-4}\,m^2\,s^{-2}$) (Figures 2e and 4e). The salinity maximum remains well defined until February–March in the simulated LCE. During this period, the mixed-layer deepens and reaches the upper bound of the maximum salinity core of the Caribbean SUW (isohaline of 36.6 in Figure 4b).

The period during which the salinity maximum started to erode (around December) coincides with strong wind stress (Figure 4e; dashed black line) and surface cooling due to negative air-sea fluxes (Figure 4e; solid blue line). The largest net cooling of $-300\,W\,m^{-2}$ and strongest wind stress ($>0.11\,N\,m^{-2}$) occurred in December, at the beginning of the subsurface salinity erosion. In response to this surface cooling, the mixed layer progressively deepens and reaches its maximum depth of ~200 m by the end of February, and the high-salinity core of the Caribbean SUW is completely eroded. At this time, the LCE is located near the western Gulf but still far from interacting with any continental slope (Figure 4a). The mixing of SUW with surface waters, together with the mixed-layer water mass transformation occurring in winter (middle December to March) lead to the formation of GCW (with salinity weaker than 36.6 at ~22°C; Figures 4b and 4d).

During most of spring and summer (April to August), the net air-sea heat fluxes turn positive, and the wind stress weakens (Figure 4e), so the upper ocean restratifies and the mixed-layer shallows to about 30 m (Figures 4b and 4d). The next summer (June to August), the evaporation exceeds the precipitation and hence concentrates seawater salt content (Figure 5), causing the salinization of the shallow mixed-layer (Figures 4b and 5a). Both temperature and salinity at the LCE's core follow a seasonal cycle in the upper ocean (0–50 m) with warmer and saltier (cooler and fresher, respectively) temperatures (Figure 4d) and salinities (Figures 4b and 5a) in summer (winter). The mixed-layer depth also follows a seasonal cycle, which is in qualitative agreement with the convective depth (h_c) estimated as a function of net heat fluxes and the local rate of change of temperature (Figure 4e; solid blue line) as

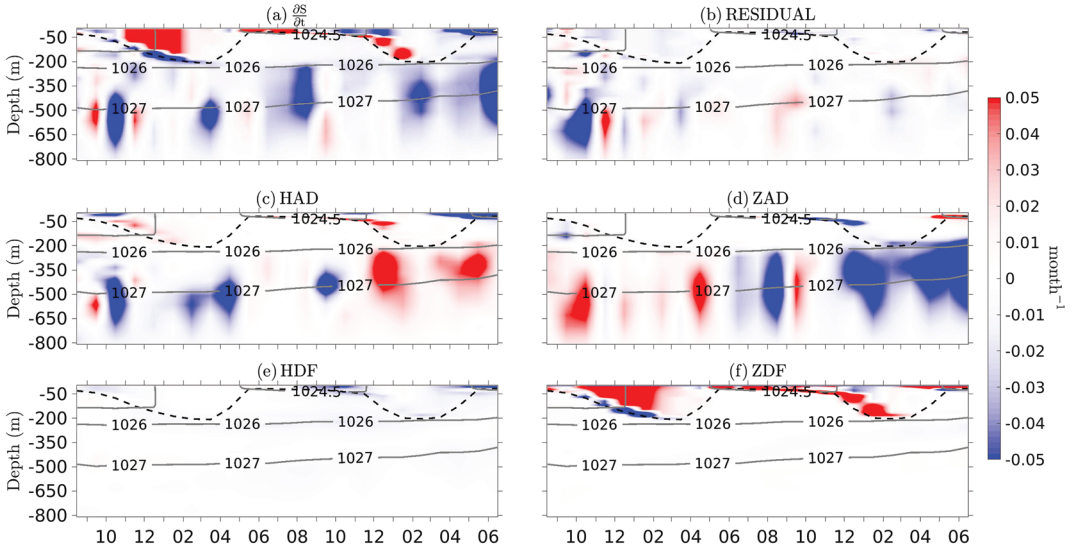

Figure 6. Salt budget inside the longest-lived numerical LCE (in month^{-1}). Time evolution of (a) local rate of change of salinity ($\partial S/\partial t$; month^{-1}), (b) residual (*Res*), (c) horizontal advection (*HAD*), (d) vertical advection (*ZAD*), (e) horizontal diffusion (*HDF*), and (f) vertical diffusion (*ZDF*) within a 30 km radii from the center of the numerical LCE as a function of depth. The dashed black lines in (a)–(f) represent the mixed-layer depth and the gray thick contours are the isopycnals of 1,024.5, 1,026, and 1,027 kg m^{-3}.

$$h_c = \frac{Q_{net}}{\rho C_p \partial T/\partial t}, \tag{4}$$

where Q_{net} is the net heat flux and T is the mixed-layer temperature. Interestingly we note that the mixed-layer deepening (slope of black dashed line in Figure 4b) is 2.5 times much faster during the second winter compared to the first winter. This is most probably due to the lower heat content (see section 5) and much more stratified upper ocean conditions observed in "mature" summer LCEs (Figure 4d). During the second winter of the eddy life cycle, no significant dilution of subsurface salinity is observed since (positive) subsurface vertical gradients of salinity were eroded during the first winter (Figure 4c).

The salt budget averaged over the LCE is now used to identify which of the forcing terms most likely contribute salt dilution in the upper 250 m (Equation 3). We separate the analysis into two different layers: (i) from 0–50 m and (ii) from 50–250 m. The seasonal evolution of each term of the salt budget in the two studied layers are shown in Figures 5 and 6.

In the upper 50 m (Figure 5), the seasonal salinity is mainly explained by the sum between the freshwater terms (FLX) and vertical salinity diffusion terms (ZDF) (Equation 3). The evaporation is always larger than precipitation but in winter the salinization effect is stronger because of the lack of precipitations over the GoM. The ZDF term extracts salinity from the upper 50 m and compensates largely the FLX term. The contribution of the advection terms (HAD and ZAD) and the horizontal diffusion (HDF) in this layer is negligible during most of the time but become the most important terms at the end of the LCE life cycle.

The salt tendency in the 50–250 m layer (Figure 6a) is mainly explained by the vertical salinity diffusion term (ZDF; Figure 6f). In deeper layers (below the isopycnal of 1,026 kg m^{-3}), the advection of salinity is the most important term and both the horizontal advection (HAD; Figure 6c) and vertical advection (ZAD; Figure 6d) largely cancel each other. The contribution of the horizontal salinity diffusion (HDF; Figure 6e) on the salt trend is negligible. Consistent with the deepening of the mixed layer in autumn (Figure 4b) and the enhanced vertical salinity gradient at the base of the mixed layer (Figure 4c), the vertical diffusion increases the salinity (ZDF > 0) in the mixing layer and decreases just below within a narrow layer of negative vertical salinity diffusion (Figure 6f).

During late first winter and spring the salinity rate of change within the deep mixed layer is negligible ($\frac{\partial S}{\partial t} \simeq 0$; Figure 6a), in agreement with homogeneous upper ocean salinity (Figure 4b) and temperature

Table 2
Total Number of LCEs Used to Compute the LCE Composites

Season								Characteristics			
Spring	Summer	Autumn	Winter	Spring	Summer	Autumn	Winter	Radius($\mathscr{R}$; km)	S_{max}	Z_{max}(m)	t_I(%)
# 1(36.86)	# 1(36.84)	# 1(36.79)	# 1(36.73)					156.0 ± 29.4	36.86	222	49.23
# 2(36.81)	# 2(36.77)	# 2(36.71)	# 2(36.67)					141.3 ± 24.7	36.81	222	27.87
	# 3(36.82)	# 3(36.78)	# 3(36.73)	# 3(36.65)	# 3(36.64)			180.2 ± 32.1	36.82	222	43.66
	# 4(36.87)	# 4(36.84)	# 4(36.79)	# 4(36.71)				126.5 ± 26.7	36.88	201	33.33
	# 5(36.76)	# 5(36.71)	# 5(36.66)	# 5(36.59)				130.3 ± 22.7	36.76	222	0
		# 6(36.73)	# 6(36.66)	# 6(36.57)	# 6(36.53)	# 6(36.51)	# 6(36.48)	125.63 ± 38.6	36.73	200	50.45
		# 7(36.79)	# 7(36.76)	# 7(36.69)	# 7(36.65)	# 7(36.63)	# 7(36.60)	149.8 ± 44.2	36.79	222	55.88
		# 8(36.92)	# 8(36.84)	# 8(36.72)	# 8(36.69)	# 8(36.65)	# 8(36.63)	155.7 ± 31	36.92	246	60.36
		# 9(36.82)	# 9(36.76)	# 9(36.67)	# 9(36.63)	# 9(36.62)		131.0 ± 26.7	36.82	164	14.68
		# 10(36.83)	# 10(36.81)	# 10(36.74)				111.3 ± 19.1	36.83	201	0
			# 11(36.88)	# 11(36.81)	# 11(36.77)	# 11(36.75)		173.4 ± 52.1	36.88	182	51.56
			# 12(36.81)	# 12(36.74)	# 12(36.69)	# 12(36.64)		125.0 ± 20.8	36.81	222	10
			# 13(36.92)	# 13(36.81)	# 13(36.74)	# 13(36.67)	# 13(36.66)	144.7 ± 31.8	36.92	222	35.56
			# 14(36.88)	# 14(36.80)	# 14(36.75)	# 14(36.70)		153.1 ± 33.9	36.88	223	48.48
			# 15(36.88)	# 15(36.79)	# 15(36.75)			173.2 ± 22.5	36.88	222	33.33
			# 16(36.81)	# 16(36.73)	# 16(36.66)	# 16(36.63)		144.3 ± 13.2	36.81	182	17.92

Note. Symbol # indicates the number of the eddy detached from the LC and (within parenthesis) is reported the averaged salinity maximum as function of the season. For example, Eddy #2 was shed on the first Spring (March) and lasted for one year. Notice that all sixteen LCEs lasted more than 180 days, and hence, all of them experienced one winter away from the Gulf continental slope, with the exception of LCEs #1 and #2. Monthly time averaged for the LCEs' radius ($\mathscr{R}$) ± 1 standard deviation (km), maximum salinity values (S_{max}), their location (Z_{max}; m), and the % interaction's time of the LCEs with the western Gulf continental slope (t_I) is shown for reference. The t_I is defined by the ratio between the time period when the periphery of the eddy (computed following Chaigneau et al., 2009) crosses over the isobath of 500 m and the total LCE lifetime.

(Figure 4d) and reduced vertical gradients of salinity (Figure 4c). During the second summer, the seasonal thermocline located near 30 m separates the shallow mixed layer from the well-mixed thermostad layer (Figures 4b and 4d). Consequently, the salinity in the shallow mixed-layer increases due to increased evaporation (Figure 5b). The next late autumn and winter, the salinity decreases in the upper first ∼30 m (Figure 5a) and increases below (Figure 4b), in agreement with the enhancement of the wind stress and negative total heat fluxes (Figure 4e).

The residual term *Res* is small from surface down to 250 m (Figures 5b and 6b) and larger below the 1,027 kg m^{-3} isopycnal, specially during the first months of the eddy life cycle; afterward the term is small through

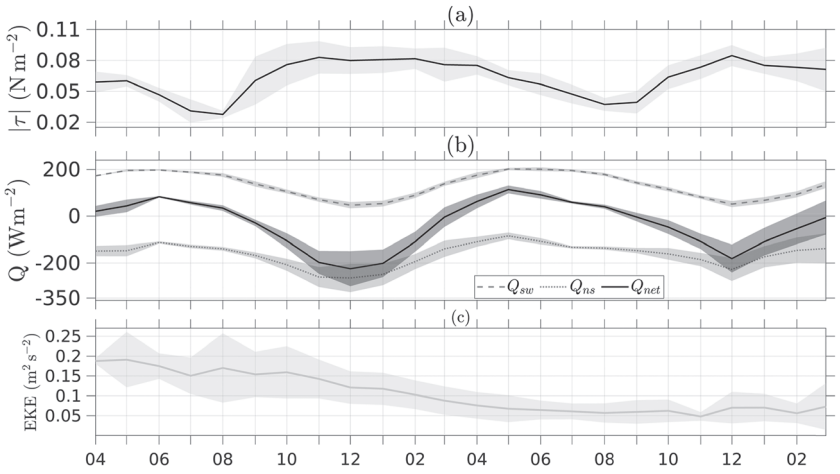

Figure 7. Monthly composites of the time evolution of sixteen LCEs of (a) wind stress ($|\tau|$ N m^{-2}), (b) heat fluxes (W m^{-2}), where Q_{sw} (gray dashed line), Q_{ns} (gray dash-dotted line), and Q_{net} (black line) are the solar, nonsolar, and net heat fluxes, respectively, and (c) eddy kinetic energy (EKE, m^2 s^{-2}). Shaded gray areas refer to the (intereddy) standard deviation.

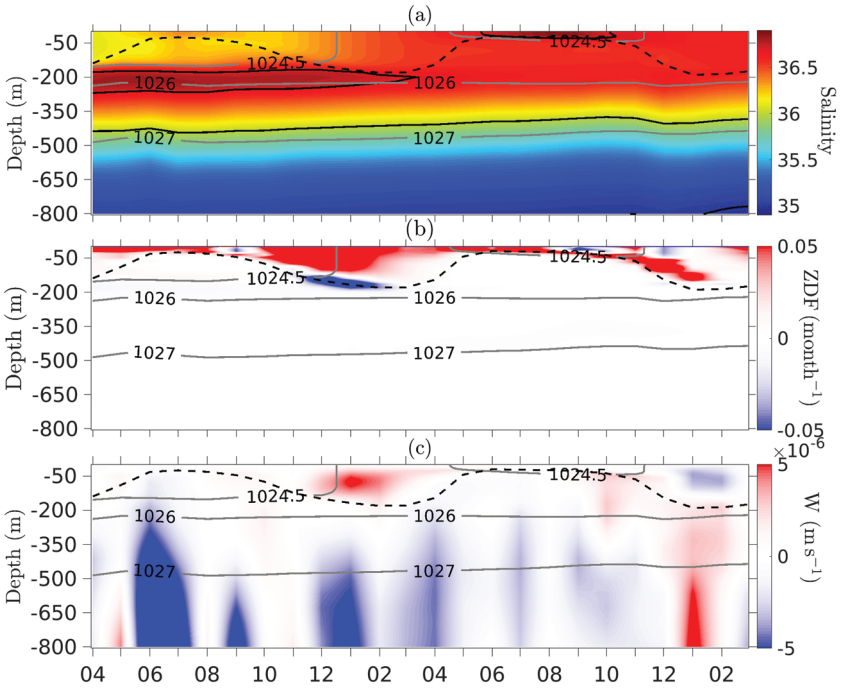

Figure 8. Monthly composites of the time evolution of 16 LCEs of (a) salinity, (b) vertical salinity diffusion (month^{-1}), and (c) vertical velocity (m s^{-1}). Black thick contours in (a) are the isohalines of 36 and 36.7; the dashed black lines in (a)–(c) represent the mixed-layer depth, and the gray thick contours are the isopycnals of 1,024.5, 1,026, and 1027 kg m^{-3}.

the whole water column indicating a nearly closed salt budget within the eddy core during most of the LCE's life span.

4.2. Composite Analysis of the Modeled LCEs

In order to verify whether the fate of LCE Poseidon and the LCE case study described in the previous section, are statistically relevant, we now perform a composite analysis of the 16 long-lived LCEs shed by the LC during the 20 year long simulation. Detachments of the 16 numerical LCEs mostly occurred on December (37.5%) and September (31.25%) (Table 2). Hall and Leben (2016), using reanalyzed satellite imagery, also found that the separation events of LCEs are more frequent in August (20%) and September (20%) (and February–March; 33%); however, none of 30 LCEs they studied were shed in December. Hence, the composite analysis of the numerical LCEs shown here may overestimate the salinity erosion during the first winter. The composite seasonal evolution has been computed for wind stress, heat fluxes and EKE (Figure 7), and salinity, vertical salinity diffusion, and vertical velocity (Figure 8) within the core of the LCEs. The same results hold for the composite analyses if we use a 60 km radii to define the core of the LCEs (not shown). The average is performed monthly along a climatological year starting with the LCEs separated in March. For example, the vertical salinity structure of five LCEs contributed to the August monthly ensemble: Two LCEs shed on April (#1 to #2) and three (#3 to #5) in June (Table 2). This methodology is more convenient to isolating the seasonal physical processes that contribute to the salt dilution. By using a discriminator

Table 3
Maximum Temperature and Salinity Anomalies, Volumetric Available Heat Anomaly (AHA), and Volumetric Available Salt Anomaly (ASA) for the Sampled Young Poseidon (Mission 0003) and for the Numerical Young LCE Composite

	T (°C)/S anomalies	AHA (J)	ASA (kg)
Glider observations (Mission 623–0003)	9.7/1.22	1.1×10^{21}	2.1×10^{13}
Young eddy composite	4/0.4	6.55×10^{19}	1.41×10^{12}

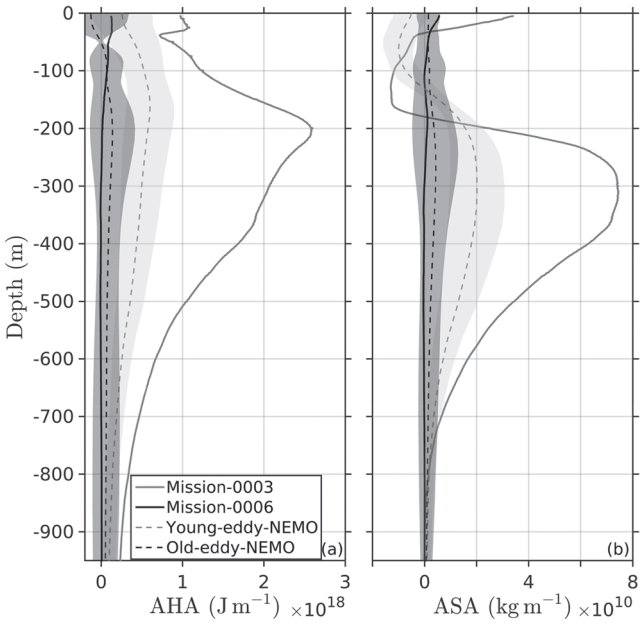

Figure 9. Composites of Available Heat Anomaly (AHA) and Available Salt Anomaly (ASA) computed from 16 numerical eddies during the first month since detachment from the Loop Current (LC) (young-eddy-NEMO) and during the last month before dissipation (old-eddy-NEMO). (a) Composite of the AHA (J m^{-1}) as a function of depth with superimposed the AHA for young (Mission 0003) and old (Mission 0006) Poseidon for reference. (b) Composite of the ASA (kg m^{-1}) as a function of depth. Lines styles are indicated in legend. Shaded gray areas indicate the (intereddy) standard deviation.

based on the elapse time since detachment from the LC (or 2° longitudinal bands), the construction of the composites would average LCEs with different salinity vertical structure. Notice that since most of the numerical eddies were released in autumn and winter (see Table 2), the vertical diffusion of salinity also drives erosion of the subsurface salinity maximum (and GCW formation) during the first 180 days after detachment (not shown). In the context of erosion of the SUW of this paper, we find more convenient to define the age of the LCEs as a function of the strength of the subsurface salinity maximum. Young (old) eddies have a strong (weak) signal of the SUW.

Details on the characteristics of the LCEs detached during the 20 year run are shown in Table 2. Notice that only two numerical LCEs separated in spring and traveled across the Gulf basin with the SUW core largely intact. The other fourteen LCEs reach the western Gulf slope with significantly diluted high-salinity cores of the SUW (not shown). Consequently, slope-eddy interactions may have little impact on our composite analysis of the SUW dilution despite that most of them (i.e., 14 over 16) did interact for a significant portion of their lifetime (see Table 2; t_I). Young LCEs (young stage) show a strong subsurface signature of the Caribbean SUW with maximum salinity above 36.7 located between 180 and 250 m (Figure 8a) and with intense EKE (0.2 m^2 s^{-2} $\pm$ 0.05 m^2 s^{-2}; Figure 7c). This high-salinity core inside the LCEs in the eastern GoM is always present regardless of the season of the year they are detached (not shown) and they present relatively homogeneous properties in terms of salinity maximum and depth (Table 2).

The composites of salinity, vertical diffusion of salinity, and vertical velocity are computed using the whole data set of 16 numerical LCEs (Figure 8). If we only considered data located to the east of 94 W (not shown), similar composites are obtained, indicating that the effect of eddy-slope interactions on SUW dilution is of second order in our study. The composite analysis confirms that dilution of the high-salinity core (erosion stage) starts on average on late autumn and continues until late winter (see isohaline of 36.7 in Figure 8a), the season with intense wind stress and the largest net negative air-sea heat fluxes (Figures 7a and 7b). The nonsolar air-sea heat fluxes (Q_{ns} term including longwave infrared radiation, latent and sensible air-sea fluxes) and the shortwave radiation (Q_{sw}) have a clear seasonal cycle with maxima during summer-spring and minima during winter associated with enhanced surface cooling due to latent and sensible heat fluxes. These large winter coolings are due to the passage of intense cold fronts over the GoM (Figure 7a). Notice that the resulting composite net air-sea heat fluxes reach -200 W m^{-2} in December (Figure 7b). Between late autumn and winter, convection due to surface buoyancy loss in response to the surface cooling, increases and decreases the salinity in the upper 200 m and below, respectively (Figure 8b). By spring, the high-salinity core of the LCEs is completely eroded (mature stage), and the salinity maximum decreases to 36.5. Winter convection drives a vertically homogeneous upper layer (thick mixed-layer) with nearly constant salinity (Figure 8a) and temperature (not shown). This homogeneous layer or mode water is isolated from the atmosphere by the seasonal thermocline on summer and is the precursor of the GCW.

5. Available Heat and Salt Anomaly Content Into the LCEs

The LCEs have significant temperature-salinity anomalies that are redistributed into the western GoM, due to the westward translation. The analyses with gliders observations and numerical data from NEMO can be used to quantify the total content of available heat and salt anomalies that the LCEs carry during their journey to the west. Consistent with Meunier et al. (2018), the vertically integrated AHA and ASA, from surface to the base of the LCE Poseidon (~1,000 m), during Mission 0003 was of 1.1×10^{21} J (this value is not correct in Meunier et al. (2018) and should be increased by a factor of 100) and 2.1×10^{13} kg (Table 3), associated

with mean T/S anomalies of 6.44°C/0.75 at 200/310 m (not shown). These AHA and ASA volumetric contents are much larger than the ones associated with subsurface anticyclonic eddies of the Peru-Chile Current System (8.7×10^{18} J and 23.8×10^{10} kg; Chaigneau et al., 2011), the California Current (0.36×10^{18} J and 1.58×10^{10} kg Pelland et al., 2013), and the Northeastern subtropical Atlantic (2.9×10^{18} J and 14.3×10^{10} kg; Barceló-Llull et al., 2017). The difference in contents within the LCEs versus the Pacific Ocean and Northeastern subtropical Atlantic anticyclonic eddies is associated with their respective sizes and T/S anomalies. In particular, Poseidon was a huge and intense LCE with a mean radii of 180 km, vertical extension of 1,000 m, and maximum T/S anomalies in their core of 9.7°C/1.22 that largely exceed the size and anomalies of the eddies found in other regions of the world ocean (Barceló-Llull et al., 2017; Chaigneau et al., 2011; Pelland et al., 2013).

The higher AHA and ASA volumetric contents suggest that the LCEs contribute significantly to the warming and salinization of the GoM. This contribution may vary depending on the individual eddy. Therefore the model is used to study the intereddy variability of the AHA and ASA content they carry as a function of depth (Figure 9). The AHA and ASA volumetric content for young (recently detached and with strong signal of the SUW) composite eddy are $6.55 \pm 3.58 \times 10^{19}$ J and $1.41 \pm 1.09 \times 10^{12}$ kg, respectively. These values of integrated AHA and ASA are up to 2–3 times weaker in comparison with the ones obtained for Poseidon (Figure 9), due to the weaker T/S anomalies (~4°C/~0.4) than LCE Poseidon. However, it should be emphasized again that Poseidon was an exceptional, huge, and intense, LCE. Composite LCEs T/S anomalies computed using a combination of mooring and altimetry data are of ~3°C/~0.3 (not shown), in agreement with composite NEMO LCEs T/S anomalies.

6. Discussion and Concluding Remarks

LCEs transport warm and saltier Caribbean SUW to the western GoM and play a significant role in the heat and salt budgets (Meunier et al., 2018) and modulate water mass distribution across the central and western GoM (Hamilton et al., 2018; Portela et al., 2018). A recent work by Meunier et al. (2020) reports that most of the LCEs decay occurs in the central GoM through submesoscale diffusive processes at scales smaller than 0.25° and before the eddy-eddy interactions occur. Meunier et al. (2019), using glider observations across the LCE Poseidon, show a new submesoscale mechanism for LCEs dissipation: that is, layering. Thin layers of temperature and salinity anomaly were observed at zones of high velocity shear at the periphery and below the LCE Poseidon, which may play an important role for the vertical tracer cascade. The LCEs ultimately diffuse the total salt and heat contents they carry toward surrounding GoM waters over the western slope (i.e., at the eddy graveyard).

Understanding the erosion of the water masses contained inside the LCEs and their transformation is important. Literature points to three main mass exchange processes between the LCEs and the surrounding waters: (submesoscale) lateral diffusivity (Meunier et al., 2019, 2020), viscous decay and slope interactions (Biggs, 1992; Vukovich & Waddell, 1991; Vidal et al., 1992, 1994), and eddy-eddy interactions that split, strip, and squeeze the LCEs (see Lipphardt et al., 2008, and references therein). Following Flierl (1981), SUW in isolated LCEs would be maintained in the eddy; that is, the mass exchange with surrounding waters would be negligible, if the LCEs translation velocity is smaller than LCEs swirl velocity. The opposite may occur approaching the eddy graveyard region when the LCEs spin down and their swirl velocities weaken. Because LCEs are not isolated, mixing events, and heat (and salt) erosion due to the interaction of the LCEs with the ambient submesoscale turbulence (Meunier et al., 2019, 2020) and mesoscale (Lipphardt et al., 2008) have been observed in the interior GoM before LCEs reach the eddy graveyard.

Among the observations reported in Meunier et al. (2018, 2019), the LCE Poseidon was surveyed until it reached the eddy graveyard along three more glider missions. A detailed check of altimetry showed that LCE Poseidon did not interact with other mesoscale eddies during its westward journey, indicating that there was negligible horizontal exchange of mass during Mission 0003. Small cyclonic eddies are continuously interacting with the large LCE Poseidon but they may have little effect on the mass exchange with the core of the eddy, as defined in this work. On mid-December 2016 (beginning Mission 0004), however, the southern portion of the LCE Poseidon was pinched off by two cyclonic eddies near [22°N, 94°W] and a new anticyclonic eddy formed to the northeast. Nevertheless, the core of the LCE Poseidon remained

unaltered until early January 2017 when the LCE Poseidon started its interaction with the western Gulf continental slope, presumably driving SUW dilution through lateral mixing. The large cancelation between horizontal and vertical advection of salinity and weak contribution of horizontal diffusive processes in the salt budget before the LCEs reach the western Gulf slope, support that most of the simulated LCEs conserve mass within their cores, defined here as a circle of 30 km radii centered at the core of the LCEs.

Salinity observations show the dilution of the core of the Caribbean SUW across the Gulf (or over the time that elapses) but with the largest erosion occurring during winter 2016 between Missions 0003 and beginning of 0004. The evolution of the salinity distribution in the longest-lived numerical eddy and the eddy composite analysis reinforces this picture of enhanced dilution of the SUW high-salinity core during the first winter of the LCE life cycles. With the available data, the most important physical process that controls the LCEs' core salinity budget is the vertical salinity diffusion which is in phase with enhanced winter wind stress, and associated negative heat fluxes, due to the passage of cold fronts over the GoM and strong (positive) vertical salinity gradient at the base of the thermostad. The salinity stratification in the LCEs' core is determined by the formation processes of the North Atlantic Subtropical Water in the Northwest North Atlantic and water mass transformation during its advection westward through the Lesser Antilles, Caribbean Sea, and Yucatan Channel. Regardless of the intrinsic variability of the water mass formation in the North Atlantic, the salinity LCE composite analysis shows a coherent vertical structure with a subsurface 100 m layer of high salinity (>36.7) centered near the isopycnal of 1,026 kg m^{-3} and fresher water mass in the upper ocean. Qualitatively, based on numerical results, the vertical structure of salinity is similar from one eddy to another, regardless of the month of the year, the LCEs were detached from the LC.

The coexistence during the first winter of both, strong wind stress and strong salinity vertical gradient in young LCEs, increases the efficiency of the vertical diffusion to incorporate saltier water into the mixing-layer (i.e., the layer were convective mixing is currently active) and fresher water into the SUW high-salinity core, reducing the subsurface vertical salinity gradients through erosion of the latter. Concomitant deepening of the mixed-layer and homogenization of the salinity in the upper ocean prevents further turbulent flux of salt into the thermostad, through vertical diffusion, even if the atmospheric forcing increases again during the second autumn and winter.

Camara et al. (2015) and Da-Allada et al. (2017) concluded that the mixed-layer salinity change in the equatorial tropical Atlantic is also dominated by vertical salinity diffusion. However, contrary to our work, the seasonal cycle of vertical salinity diffusion is in phase opposition with the one of the vertical diffusion coefficient (or wind stress). The differences are due to the seasonality of the vertical salinity stratification and vertical shear of the regional currents. Strong salinity stratification peaks in May-April due to upper-ocean freshening by strong precipitation (Camara et al., 2015) and advection of low-salinity water from the Gulf of Guinea (Da-Allada et al., 2017). Similarly, large vertical shear resulting from the strong westward South Equatorial Current flowing above the (subsurface) eastward Equatorial Under Current is strong in spring (Camara et al., 2015; Da-Allada et al., 2017). In the LCEs the vertical salinity gradient at the base of the thermostad does not follow a seasonal cycle and its magnitude depends on how many months the LCEs have spent in the GoM under the effect of the atmospheric forcing, eddy-eddy, and topographic interactions. Since the salt budget is computed in the core of the LCEs (low-velocity region), no expected source of mesoscale vertical shear is available for mixing. Another possible source of shear instability is the vertical shear induced by near-inertial oscillations trapped in the mixed layer. Enhanced wind power input to mixed-layer near-inertial oscillations in the GoM occurs due to the passage of cold fronts in autumn/winter and hurricanes in summer. However, inside anticyclonic vorticity (i.e., LCEs) large vertical dispersion of near-inertial energy downward takes place (Kunze, 1985; Pallàs-Sanz et al., 2016), which reduces the amount of near-inertial kinetic energy available for vertical entrainment at the base of the mixed layer (Jaimes et al., 2011). Consequently, this mixing mechanism does not account for the subsurface erosion of the SUW high-salinity core but could be eventually important during summer, because of the coalescence of hurricane winds and shallow mixed layer.

Below the isopycnal of 1,026 k m^{-3} the advective processes fully control the rate of change of salinity $\partial S/\partial t$. The vertical (horizontal) advection of salinity is positive (negative) during most of the LCEs lifetime and negative (positive) at the eddy graveyard. Vertical velocity in the core of the LCEs can arise through eddy pumping mechanism (Klein & Lapeyre, 2009). If an anticyclonic eddy decays (strengthens), density

conservation equation states that positive (negative) vertical velocity may occur inside the eddy. During most of the lifetime of the LCEs, negative vertical gradients of salinity year-round ($\partial S/\partial z<0$) together with downwelling ($w<0$; Figure 8c) salinizes the interior ocean through positive vertical advection of salinity ($w\partial S/\partial z>0$). At the eddy graveyard, the opposite occurs with interior ocean freshening through negative vertical advection of salinity ($w\partial S/\partial z<0$) due to eddy decay and positive eddy pumping ($w>0$; Figure 8c). Typically, horizontal and vertical advection largely cancel each other indicating volume salinity conservation within the LCEs' core, that is, $\partial S/\partial t+\mathbf{u}\cdot\nabla S=0$ (where $\mathbf{u}=(u,v,w)$). However, there are specific periods within the life span of the LCEs, which the addition of both contributions mostly results in a loss of salt ($\partial S/\partial t<0$) driven by horizontal advection, during most of the lifetime of the LCEs, and by vertical advection at the eddy graveyard, suggesting net mass exchange with surrounding waters (see, e.g., Lipphardt et al., 2008).

The contribution of the westward propagating LCEs in modulating the GoM's heat and salt content is very important due to the large T/S anomalies they carry relative to other oceanic eddies. Assuming that all the mean volumetric heat and salt content transported by the NEMO LCE composite, $AHA_{\mathscr{V}}=6.55\pm3.58\times10^{19}$ J and $ASA_{\mathscr{V}}=1.41\pm1.09\times10^{15}$ g is diffused in the upper 1,000 m depth, the temperature and salinity of the GoM would increase by $\Delta T=AHA_{\mathscr{V}}/C_p\mathscr{M}=0.15\pm0.085\times10^{-1}$ °C and $\Delta S=ASA_{\mathscr{V}}/\mathscr{M}=1.41\pm1.1\times10^{-3}$, respectively, here $\mathscr{M}=1\times10^{18}$ kg is the total mass in the entire basin from surface to 1,000 m depth. These values are smaller than the increase that would produce mixing Poseidon's heat and salt content (2.4×10^{-1} °C and 2.3×10^{-2}) in the upper 1,000 m of the GoM because LCE Poseidon was an exceptional eddy with huge excess of heat and salt. Moreover, since NEMO consistently underestimates the salinity and heat contents of numerical LCEs, their contribution to Gulf's salt and heat budget might be also underestimated.

Although the study of the heat and salt budget in the GoM is beyond the scope in this work, we conclude that winter convection inside the core of young LCEs is an effective mechanism for erosion of the SUW and production of GCW that ultimately will be released into the GoM when the LCEs dissipate. In addition, this vertical process of erosion of salinity may work counteracting the loss of salt driven by (submesoscale) lateral diffusion (Meunier et al., 2019, 2020). Erosion of the subsurface salinity maximum by vertical mixing reduces the horizontal gradients of salinity and the effect of the submesoscale turbulence surrounding the LCEs. Therefore, LCEs separated just before winter begins may decay slower (see, e.g., LCEs #6, #7, and #8, in Table 2).

An important limitation of the composite analysis is the length of the numerical record (20 year) and the number of long-lived LCEs considered in the analysis. Unambiguously, we have only selected the LCEs that lasted longer than 180 days and without considering splitting/merging processes, which produced sixteen realizations from the original 34. The production of GCW within a particular LCE might differ significantly from one to another because of the strong influence of the month of detachment. LCEs separated from the LC in late winter and spring will not experience a winter before reaching the western Gulf continental slope. Vukovich (2007) indicates that about 44% of the LCEs observed between 1972 and 2003 in the GoM separated in late winter and spring period (i.e., February, March, April, and May), Hall and Leben (2016) shows that about 30% of the LCEs observed between 1993 and 2012 in the GoM were separated during summer, 30% in autumn, 23% in spring, and 17% in February, and Hamilton et al. (2018) found that 10–30% of the ARGO float salinity profiles on the western GoM still have a large SUW salinity maximum (~36.6) suggesting that a similar percentage of LCEs were separated in late winter and spring period. In the data set shown here the ~19% of the long-lived LCEs were released in summer, the ~31% in autumn, but none in late winter (i.e., February). Hence, the composite analysis is certainly biased toward the averaged salinity response within LCEs that experience the whole winter away from the boundaries of the GoM. Further work will be oriented to understand the complex interactions of LCEs with the western Gulf slope (Vukovich & Waddell, 1991) and how they modulate the vertical salinity structure inside LCEs.

Data Availability Statement

Glider's data from GMOG can be freely visualized at the GMOG's webpage (https://gliders.cicese.mx/) and distributed on demand for reviewing purpose. The altimeter products were produced by SSALTO/Duacs, processed and distributed by Copernicus Marine and Environment Monitoring Service (CMEMS; https://www.copernicus.eu/en).

Acknowledgments

This study is a contribution of the Consorcio de Investigación del Golfo de México (CIGoM) through Project 201441 "Implementación de redes de observación oceanográficas (físicas, geoquímicas, y ecológicas) para la generación de escenarios ante posibles contingencias relacionadas a la exploración y producción de hidrocarburos en aguas profundas del Golfo de México" funded by the Hydrocarbons trust from the Secretaría de Energía (SENER) and Consejo Nacional de Ciencia y Tecnología (CONACyT). R. Sosa-Gutiérrez was co-funded via two doctoral grants from the CONACyT and CIGoM. The glider missions were designed and performed by the Grupo de Monitoreo Oceanográfico con Gliders (GMOG). We acknowledge the GMOG's technicians involved in the operations of installation and recovery of the gliders during Missions 0003–0006. We are thankful to Dr. Meunier for fruitful discussions and two anonymous reviewers for their suggestions and valuable comments on the manuscript.

References

Akhil, V. P., Durand, F., Lengaigne, M., Vialard, J., Keerthi, M. G., Gopalakrishna, V. V., et al. (2014). A modeling study of the processes of surface salinity seasonal cycle in the Bay of Bengal. *Journal of Geophysical Research: Oceans*, *119*, 3926–3947. https://doi.org/10.1002/2013JC009632

Barceló-Llull, B., Sangrà, P., Pallàs-Sanz, E., Bartond, E., Estrada-Allis, S., Martínez-Marreroa, A., et al. (2017). Vertical structure of mesoscale eddies in the eastern South Pacific Ocean: A composite analysis from altimetry and Argo profiling floats. *Deep Sea Research Part I: Oceanographic Research Papers*, *124*, 126–139. https://doi.org/10.1016/j.dsr.2017.03.012

Biggs, D. C. (1992). Nutrients, plankton, and productivity in a warm-core ring in the western Gulf of Mexico. *Journal of Geophysical Research*, *97*, 2143–2154.

Brooks, D. A. (1984). Current and hydrographic variability in the northwestern Gulf of Mexico. *Journal of Geophysical Research*, *89*, 8022–8032.

Camara, I., Kolodziejczyk, N., Mignot, J., Lazar, A., & Gaye, A. T. (2015). On the seasonal variations of salinity of the tropical Atlantic mixed layer. *Journal of Geophysical Research: Oceans*, *120*, 4441–4462. https://doi.org/10.1002/2015JC010865

Chaigneau, A., Eldin, G., & Dewitte, B. (2009). Eddy activity in the four major upwelling systems from satellite altimetry (1992–2007). *Progress in Oceanography*, *83*, 117–123.

Chaigneau, A., Le Texier, M., Eldin, G., Grados, C., & Pizarro, O. (2011). Vertical structure of mesoscale eddies in the eastern South Pacific Ocean: A composite analysis from altimetry and Argo profiling floats. *Journal of Geophysical Research*, *116*, C11025. https://doi.org/10.1029/2011JC007134

Chelton, D. B., deSzoeke, R. A., Schlax, M. G., Naggar, K. E., & Siwertz, N. (1998). Geographical variability of the first baroclinic Rossby radius of deformation. *Journal of Physical Oceanography*, *28*(3), 433–460.

Cooper, C., Forristall, G. Z., & Joyce, T. M. (1990). Velocity and hydrographic structure of two Gulf of Mexico warm-core rings. *Journal of Geophysical Research*, *95*(C2), 1663–1679.

Da-Allada, C. Y., Alory, G., Du Penhoat, Y., Kestenare, E., Durand, F., & Hounkonnou, N. M. (2013). Seasonal mixed-layer salinity balance in the tropical Atlantic Ocean: Mean state and seasonal cycle. *Journal of Geophysical Research: Oceans*, *118*, 332–345. https://doi.org/10.1029/2012JC008357

Da-Allada, C. Y., Jouanno, J., Gaillard, F., Kolodziejczyk, N., Maes, C., Reul, N., & Bourlès, B. (2017). Importance of the Equatorial Undercurrent on the sea surface salinity in the eastern equatorial Atlantic in boreal spring. *Journal of Geophysical Research: Oceans*, *122*, 521–538. https://doi.org/10.1002/2016JC012342

Dai, A., & Trenberth, E. (2002). Estimates of freshwater discharge from continents: Latitudinal and seasonal variations. *Journal of Hydrometeorology*, *3*, 660–687.

Dong, C., McWilliams, J., & Chen, D. (2013). Global heat and salt transports by eddy movement. *Nature Communications*, *5*, 3294.

Donohue, K., Hamilton, P., Leben, R. R., Watts, D. R., & Waddell, E. (2008). Survey of deepwater currents in the Northwestern Gulf of Mexico: U.S. Dept. of the Interior, Minerals Management Service, Gulf of Mexico OCS Region, New Orleans, LA. OCS Study MMS.

Dussin, R., Barnier, B., & Brodeau, L. (2016). Up-dated description of the DFS5 forcing data set: The making of Drakkar forcing set DFS5. Grenoble, France: Lab. of Glaciol. and Environ. Geophys.

Elliott, B. A. (1982). Anticyclonic rings in the Gulf of Mexico. *Journal of Physical Oceanography*, *12*(11), 1292–1309. https://doi.org/10.1175/1520-0485(1982)012<1292:ARITGO>2.0.CO;2

Flierl, G. R. (1981). Particle motions in large amplitude wave fields. *Geophysical & Astrophysical Fluid Dynamics*, *18*, 39–74.

Foltz, G. R., Grodsky, S. A., Carton, J. A., & McPhaden, M. J. (2004). Seasonal salt budget of the northwestern tropical Atlantic Ocean along 38°W. *Journal of Geophysical Research*, *109*, C03052. https://doi.org/10.1029/2003JC002111

Garau, B., Ruiz, S., Zhang, W. F. G., Pascual, A., Heslop, E., Kerfoot, J., & Tintore, J. (2011). Thermal lag correction on slocum CTD glider data. *Journal of Atmospheric and Oceanic Technology*, *28*(9), 1065–1071.

Hall, C., & Leben, R. (2016). Observational evidence of seasonality in the timing of loop current eddy separation. *Dynamics of Atmospheres and Oceans*, *76*, 240–267. https://doi.org/10.1016/j.dynatmoce.2016.06.002

Hamilton, P., Fargion, G. S., & C., B. D. (1999). Loop Current eddy paths in the western Gulf of Mexico. *Journal of Physical Oceanography*, *29*, 1180–1207.

Hamilton, P., Leben, R. R., Bower, A. S., Furey, H., & Perez-Brunius, P. (2018). Hydrography of the Gulf of Mexico from autonomous floats. *Journal of Physical Oceanography*, *48*, 773–794.

Isern-Fontanet, J., García-Ladona, E., & Font, J. (2003). Identification of marine eddies from altimetric maps. *Journal of Atmospheric and Oceanic Technology*, *20*(5), 772–778.

Jaimes, B., Shay, L. K., & Halliwell, G. R. (2011). The response of quasigeostrophic oceanic vortices to tropical cyclone forcing. *Journal of Physical Oceanography*, *40*(10), 1965–1985.

Klein, P., & Lapeyre, G. (2009). The oceanic vertical pump induced by mesoscale and submesoscale turbulence. *Annual Review of Marine Science*, *1*, 351–375. https://doi.org/10.1146/annurev.marine.010908.163704

Kunze, E. (1985). Near-inertial wave propagation in geostrophic shear. *Journal of Physical Oceanography*, *15*(5), 544–565.

Large, W., & Yeager, S. (2004). Diurnal to decadal global forcing for ocean sea ice models: The data sets and flux climatologies. Boulder, Colo: Natl. Cent. for Atmos. Res.

Laxenaire, R., Speich, S., Blanke, B., Chaigneau, A., Pegliasco, C., & Stegner, A. (2018). Anticyclonic eddies connecting the western boundaries of Indian and Atlantic Oceans. *Journal of Geophysical Research: Oceans*, *123*, 7651–7677. https://doi.org/10.1029/2018JC014270

Lipphardt, B. L., A., P., Kirwan, A., Kantha, L., & Zweng, M. (2008). Death of three Loop Current rings. *Journal of Marine Research*, *66*, 25–60.

Madec, G., & the NEMO team (2016). Nemo ocean engine. Note du Pôle de modélisation, Institut Pierre-Simon Laplace (IPSL).

Meunier, T., Pallàs-Sanz, E., Tenreiro, M., Ochoa, J., Ruiz-Angulo, A., & Buckingham, C. (2019). Observations of layering under a warm-core ring in the Gulf of Mexico. *Journal of Physical Oceanography*, *49*(12), 3145–3162.

Meunier, T., Pallàs-Sanz, E., Tenreiro, M., Portela, J., Ruiz-Angulo, A., & Cusí, S. (2018). The vertical structure of a Loop Current Eddy. *Journal of Geophysical Research: Oceans*, *123*, 6070–6090. https://doi.org/10.1029/2018JC013801

Meunier, T., Sheinbaum, J., Pallàs-Sanz, E., Tenreiro, M., Ochoa, J., Ruiz-Angulo, A., et al. (2020). Heat content anomaly and decay of warm core rings: The case of the Gulf of Mexico. *Geophysical Research Letters*, *47*, e2019GL085600. https://doi.org/10.1029/2019GL085600

O'Connor, B. M., Fine, R. A., & Olson, D. B. (2005). A global comparison of subtropical underwater formation rates. *Deep Sea Research Part I: Oceanographic Research*, *52*, 1569–1590. https://doi.org/10.1016/j.dsr.2005.01.011

Pallàs-Sanz, E., Candela, J., Sheinbaum, J., & Ochoa, J. (2016). Mooring observations of the near-inertial wave wake of Hurricane Ida (2009). *Dynamics of Atmospheres and Oceans*, *76*, 325–344.

Pegliasco, C., Chaigneau, A., & Morrow, R. (2015). Main eddy vertical structures observed in the four major Eastern Boundary Upwelling Systems. *Journal of Geophysical Research: Oceans*, *120*, 6008–6033. https://doi.org/10.1002/2015JC010950

Pelland, N., Eriksen, C., & Lee, C. (2013). Subthermocline eddies over the Washington continental slope as observed by Seagliders. *Journal of Physical Oceanography*, *43*, 2025–2053. https://doi.org/10.1175/JPO-D-12-086.1

Portela, E., Tenreiro, M., Pallàs-Sanz, E., Meunier, T., Ruiz-Angulo, A., Sosa-Gutiérrez, R., & Cusí, S. (2018). Hydrography of the central and western Gulf of Mexico. *Journal of Geophysical Research: Oceans*, *123*, 5134–5149. https://doi.org/10.1029/2018JC013813

Qu, T., Gao, S., & Fukumori, I. (2011). What governs the North Atlantic salinity maximum in a global GCM? *Geophysical Research Letters*, *38*, L07602. https://doi.org/10.1002/jgrc.20152

Qu, T., Zhang, L., & Schneider, N. (2016). North Atlantic subtropical underwater and its year-to-year variability in annual subduction rate during the Argo period. *Journal of Physical Oceanography*, *46*, 1901–1916. https://doi.org/10.1175/JPO-D-15-0246.1

Reffray, G., Bourdalle-Badie, R., & Calone, C. (2015). Modelling turbulent vertical mixing sensitivity using a 1-D version of NEMO. *Geoscientific Model Development*, *8*, 69–86. https://doi.org/10.5194/gmd-8-69-2015

Rudnick, D. L., Gopalakrishnan, G., & Cornuelle, B. D. (2015). Cyclonic eddies in the Gulf of Mexico: Observations by underwater gliders and simulations by numerical model. *Journal of Physical Oceanography*, *45*, 313–326. https://doi.org/10.1175/JPO-D-14-0138.1

Umlauf, L., & Burchard, H. (2003). A generic length-scale equation for geophysical turbulence models. *Journal of Marine Research*, *61*, 235–265.

Vidal, V. M., Vidal, F. V., Hernández, A. F., Meza, E., & Zambrano, L. (1994). Winter water mass distributions in the western Gulf of Mexico affected by a colliding anticyclonic ring. *Journal of Oceanography*, *50*(5), 559–588. https://doi.org/10.1007/BF02235424

Vidal, V. M., Vidal, F. V., & Perez-Molero, J. M. (1992). Collision of a Loop Current anticyclonic ring against the continental-shelf slope of the western Gulf of Mexico. *Journal of Geophysical Research*, *97*, 2155–2172.

Vukovich, F. M. (2007). Climatology of ocean features in the Gulf of Mexico using satellite remote sensing data. *Journal of Physical Oceanography*, *37*, 689–707. https://doi.org/10.1175/JPO2989.1

Vukovich, F. M., & Crissman, B. W. (1986). Aspects of warm rings in the Gulf of Mexico. *Journal of Geophysical Research*, *91*(C2), 2645–2660.

Vukovich, F. M., & Waddell, E. (1991). Interaction of a warm ring with the western slope in the Gulf of Mexico. *Journal of Physical Oceanography*, *21*, 1062–1074.

Zavala-Hidalgo, J., Romero-Centeno, R., Mateos-Jasso, A., Morey, S. L., & Martínez-López, B. (2014). The response of the Gulf of Mexico to wind and heat flux forcing What has been learned in recent years? *Atmósfera*, *27*(3), 317–334.